# Single-molecule observation of the ligand-induced population shift of rhodopsin, a g-protein-coupled receptor.

AUTHOR(S):

Maeda, Ryo; Hiroshima, Michio; Yamashita, Takahiro; Wada, Akimori; Nishimura, Shoko; Sako, Yasushi; Shichida, Yoshinori; Imamoto, Yasushi

CITATION:

Maeda, Ryo ...[et al]. Single-molecule observation of the ligand-induced population shift of rhodopsin, a g-protein-coupled receptor.. Biophysical journal 2014, 106(4): 915-924

ISSUE DATE:

2014-02-18

URL:

http://hdl.handle.net/2433/185150

# Single-molecule observation of the ligand-induced population shift of rhodopsin, a G-protein coupled receptor

Ryo Maeda,[†] Michio Hiroshima,[‡,§] Takahiro Yamashita,[†] Akimori Wada,[¶] Shoko Nishimura,[‖] Yasushi Sako,[‡] Yoshinori Shichida,[†] and Yasushi Imamoto[†]

[†]Department of Biophysics, Graduate School of Science, Kyoto University, Kyoto 606-8502, Japan; [‡]Cellular Informatics Laboratory, RIKEN, 2-1 Hirosawa, Wako 351-0198, Japan; [§]Laboratory for Cell Signaling Dynamics, RIKEN Quantitative Biology Center, 6-2-3 Furuedai, Suita 565-0874, Japan; [¶]Department of Organic Chemistry for Life Science, Kobe Pharmaceutical University, Kobe 658-8558, Japan; and [‖]Cellular and Structural Physiology Institute, Nagoya University, Nagoya 464-8601, Japan.

Correspondence should be addressed to this author (imamoto@rh.biophys.kyoto-u.ac.jp).

Running head: Population shift of rhodopsin

Key words: conformational change, equilibrium, dynamics, photoreaction, metarhodopsin, two-state model.

**ABSTRACT**

Rhodopsin is a G protein-coupled receptor (GPCR), in which retinal chromophore acts as inverse-agonist or agonist depending on its configuration and protonation state. Photo-stimulation of rhodopsin results in a pH-dependent equilibrium between the active state (Meta-II) and its inactive precursor (Meta-I). Here, we monitored conformational changes of rhodopsin using a fluorescent probe Alexa594 at the cytoplasmic surface, which shows fluorescence increase upon the generation of active state, by single-molecule measurements. The fluorescence intensity of a single photo-activated rhodopsin molecule alternated between two states. Interestingly, such a fluorescence alternation was also observed for ligand-free rhodopsin (opsin), but not for dark-state rhodopsin. In addition, the pH-dependences of Meta-I/Meta-II equilibrium estimated by fluorescence measurements deviated notably from estimates based on absorption spectra, indicating that both Meta-I and Meta-II are mixtures of two conformers. Our observations indicate that rhodopsin molecules intrinsically adopt both active and inactive conformations, and the ligand retinal shifts the conformational equilibrium. These findings provide dynamical insights into the activation mechanisms of GPCRs.

## INTRODUCTION

Rhodopsin, the photoreceptor protein of retinal rod cells, is a member of G protein-coupled receptors (GPCRs) (1). GPCRs are ubiquitous membrane proteins with a seven transmembrane structure, which respond to a variety of stimuli. Unlike most GPCRs, which are activated by diffusible ligands, rhodopsin has a covalently bound retinal as an intrinsic ligand, which also functions as a light absorbing chromophore. Light absorption causes the isomerization of the inverse agonist 11-*cis*-retinal into the agonist all-*trans*-retinal (2), resulting in the formation of the active state of rhodopsin (3). In spite of the uniqueness of rhodopsin, recent progress in X-ray crystallography has revealed that the agonist-induced conformational change of rhodopsin, which involves an outward movement of helix VI, is similar to that of other GPCRs (4-7). Therefore, understanding the mechanisms of conformational changes that lead to the activation of rhodopsin could provide a new paradigm for the signaling mechanism of GPCRs.

The snapshots of resting and activated structures of GPCRs presented by X-ray crystallographic studies have provided valuable insights into the activation mechanisms of GPCRs. However, the analysis focusing on the conformational dynamics would be essential to better understand the activation mechanism of rhodopsin (8-11). In the present work, we explored the conformational dynamics of individual receptor molecules by single-molecule analysis.

Single-molecule analysis using total internal reflection fluorescence microscopy (TIRFM) has been successfully applied to analyses of intra-molecular conformational changes (12, 13) as well as inter-molecular interactions (14-16). Unlike bulk measurements, single-molecule analysis of individual molecules provides direct information about the kinetics of forward and backward reactions in an equilibrium mixture. Here we used single-molecule detection to directly monitor the conformational fluctuations between active and inactive states of rhodopsin.

Activation of vertebrate rhodopsin proceeds through the formation of an equilibrium mixture of the active state Meta-II and its inactive precursor Meta-I, which have characteristic absorption spectra owing to the protonation state of the retinal chromophore (17). Because the retinal chromophore also acts as the ligand, the protonation state of the retinal is commonly used as proxy to monitor the formation of the active state. However, crystal structures of active state of rhodopsin and other GPCRs indicate that large conformational changes occur at the cytoplasmic surface away from the ligand-binding site. In agreement with this notion, a previous study reported that Alexa594 immobilized at Cys316 on cytoplasmic helix VIII of bovine rhodopsin is sensitive to the generation of G protein activating state (Meta-II) (18).

In the present work, we examined the conformational dynamics of opsin (the ligand-free rhodopsin), dark-state rhodopsin (resting state containing 11-*cis*-retinal), as well as photo-activated rhodopsin (equilibrium mixture of Meta-I and Meta-II) by single-molecule

fluorescence measurements of Alexa594 bound to Cys316. Our single-molecule analyses strongly suggest that a rhodopsin molecule intrinsically adopts a conformational equilibrium between active and inactive conformations, which is regulated by the presence/absence, configuration, or the protonation state of the retinal chromophore.

## MATERIALS AND METHODS

### Sample preparation.

Bovine rod outer segments (ROS) were isolated from bovine retinas, and rhodopsin in ROS was labeled with Alexa594 as described previously (18). Rhodopsin labeled with Alexa594 (Rh/Alexa594) was solubilized by OG/asolectin buffer (60 mM *n*-octyl-β-D-glucoside, 1 mg/mL asolectin, 50 mM HEPES, 140 mM NaCl, pH 7.5) and purified by concanavalin A-Sepharose. The purity of rhodopsin achieved by our protocol was assessed by the optical purity index ($Abs_{280}/Abs_{500}$) of the unlabeled rhodopsin sample purified by this method, and it was typically 1.88 (Fig. S1b). The molar ratio of rhodopsin and Alexa594 in the purified Rh/Alexa594 sample was 1:0.98 based on the visible absorption spectra (Fig. S1b).

Purified Rh/Alexa594 sample, in which the molar ratio of asolectin and Rh/Alexa594 was 1300:1, was dialyzed against 500 volumes of dialysis buffer containing 140 mM NaCl and 50 mM MES (pH 6.0), 50 mM MOPS (pH 7.0), 50 mM HEPES (pH 8.0), or 50 mM CHES (pH 9.0) at 4°C in the dark for 36 hr with six buffer exchanges.

Opsin was prepared by photo-bleaching of Rh/Alexa594 in the presence of 50 mM $NH_2OH$. For TIRFM imaging of the dark-state, photoisomerization of the chromophore by excitation laser was prevented by using a retinal analog in which $C_{11}$=$C_{12}$ double bond is locked in cis configuration by a 7-membered ring (7m-Ret) (19, 20). Rh/Alexa594 regenerated with this retinal analogue (7m-Rh/Alexa594) was also purified and incorporated into asolectin liposomes. To suppress the light-induced conformational change, Rh/Alexa594 was incorporated into 1,2-dimyristoyl-phosphatidylcholine (DMPC) liposomes, in which conformational change is arrested at Meta-I stage (21). For control experiments, Rh/Alexa594 in asolectin liposome was denatured by incubating it at 90°C for 3 min. Suspensions of liposomes were centrifuged (20,400g, 20 min) and the unprecipitated liposomes in the supernatant, which contained a small number of pigment or opsin molecules, were subjected to the single-molecule analysis. Bovine rod G protein (transducin), was extracted from irradiated bovine rod outer segment membranes by adding GTP, and purified by DEAE Toyopearl 650S (Tosoh) column chromatography (22).

### Spectrophotometry.

Absorption spectra were recorded using a Shimadzu UV2450 spectrophotometer. Fluorescence spectra were recorded with a Shimadzu RF-5300PC spectrofluorometer. To

maintain the sample temperature at 6°C, an optical cell holder was connected to a Neslab RTE-7 temperature controller. The sample was irradiated with light from a 1 kW tungsten halogen lamp (Rikagaku Seiki) that had been passed through a glass cutoff filter (Y52, Toshiba). Alexa594 bound to rhodopsin was excited at 605 nm. Time-course of fluorescence changes of Alexa594 were recorded at 630 nm.

**G protein activation assay.**

GDP/GTPγS exchange by G protein transducin was examined by a radionucleotide filter-binding assay (22). All procedures were carried out at 0°C. Reaction mixtures (~125 nM pigment, 600 nM G protein, 50 mM MOPS, 140 mM NaCl, 2.25 mM $MgCl_2$, 1 mM DTT, 2 μM GDP, pH 7.0) were kept in the dark or irradiated with light generated by a 1 kW tungsten halogen lamp and Y52 filter for 30 s. The GDP/GTPγS exchange reaction was then initiated by the addition of [$^{35}$S]GTPγS (final concentration, 1 μM). After incubation for the selected time in the dark, an aliquot (20 μL) of the reaction mixture was mixed with 200 μL of stop solution (20 mM Tris/HCl, 100 mM NaCl, 25 mM $MgCl_2$, 1 μM GTPγS and 2 μM GDP, pH 7.4), and it was immediately filtered through a nitrocellulose membrane to trap [$^{35}$S]GTPγS bound to G protein. The amount of bound [$^{35}$S]GTPγS was quantitated by a liquid scintillation counter (Tri-Carb 2910 TR; PerkinElmer).

**Single-molecule imaging by total internal reflection fluorescence microscopy.**

Fluorescence of Alexa594 was observed using an inverted microscope (TE 2000, Nikon) with a 60× oil-immersion objective (ApoTIRF 60× 1.49 NA, Nikon). Fluorescence of Alexa594 was generated by 559 nm laser (WS-0559-050, 50 mW, NTT Electronics). Energy of the laser was reduced by neutral density filter (ND50). The images were acquired using an EMCCD camera (C9100-134, ImagEM, Hamamatsu Photonics) with a 345× EM gain. The image of 512×512 pixels were recorded with time resolution of 20 frame/sec and space resolution of 108 nm/pixel (2.5× relay lens) or 67 nm/pixel (4.0× relay lens). To prevent photobleaching of Alexa594 fluorophore, 2-mercaptoethanol and Trolox (6-hydroxy-2,5,7,8-tetramethylchroman-2-carboxylic acid) were added to the sample at the final concentrations of 5% (w/v) and ~1 mM, respectively. The sample dish was maintained at 6°C with an air-cooling device (Peltier-4, Taisei Denki). All sample manipulations were performed under dim red light.

**Data analyses.**

Time course of fluorescence intensity was obtained from TIRFM images by using ImageJ. Fluorescence intensity steps were detected by a laboratory-written analytical program based on hidden Markov model (23, 24) developed by LabVIEW (National Instruments). All statistical and kinetic analyses were performed with IGOR Pro 6 (WaveMetrics).

## RESULTS

### Preparation of asolectin liposomes containing rhodopsin labeled by Alexa594

In order to monitor the light-induced conformational change of rhodopsin, rhodopsin was labeled by Alexa594 at Cys316 on cytoplasmic helix VIII (Rh/Alexa594) (18). The optical purity index ($Abs_{280}/Abs_{500}$) of unlabeled rhodopsin sample prepared by our method was typically 1.88, and the molar ratio of rhodopsin and Alexa594 in Rh/Alexa594 sample was estimated to be 1:0.98 based on the visible absorption spectra (Fig. S1b). Bovine rhodopsin has two solvent-exposed Cys residues (Cys140 and Cys316), which are potentially labeled by Alexa594 (18). However, the binding efficiency for Cys140 is substantially lower than that for Cys316. Taken together, Alexa594 in our preparation is virtually homogeneous and the effect of contaminant was not taken into consideration.

Alexa594 immobilized at Cys316 shows fluorescence increase upon the generation of G protein activating state (Meta-II) (18). We prepared asolectin liposomes containing Rh/Alexa594 to disperse molecules for single-molecule analysis. Electron microscopy of these liposomes showed that our preparation was uniform and relatively small (diameter = ~70 nm, Fig. S1a). Importantly, asolectin liposomes reproduced the membrane environment of native rod outer segment (ROS) membranes, as evidenced by the pH dependent equilibrium of Meta-I/Meta-II, which is a sensitive indicator of the membrane environment (17, 25). Fig. S1c clearly shows that the pH-dependent Meta-I/Meta-II equilibrium observed in ROS membranes was preserved in asolectin liposomes, with Meta-II formation favored at lower pH having a $pK_a$ of 6.5 (25, 26). We also compared the fluorescence changes observed during photo-activation of Rh/Alexa594 in asolectin liposomes and ROS membranes. As shown in Figs. S1d and S1e, the fluorescence increase upon light irradiation of Rh/Alexa594 and its pH dependency were very similar between asolectin liposomes and ROS membranes. These findings indicate that Rh/Alexa594 incorporated into asolectin liposomes was suitable for studying the conformational change of rhodopsin by single-molecule analysis. The increase in the amount of Meta-II in the Meta-I/Meta-II equilibrium correlates well with the increase in Alexa594 fluorescence, indicating that Meta-II is mainly in a high fluorescence state, whereas dark state and Meta-I are mainly in a low fluorescence state (see below). On the other hand, fluorescence increase was reduced in DMPC liposomes, where the conformational change of photoactivated rhodopsin is arrested at Meta-I stage (Fig. S1f). At all pH, the fluorescence intensity was reduced in the presence of hydroxylamine, which converts Meta-I and Meta-II into retinal oxime and opsin (Fig. S1d, broken lines), indicating that opsin is mainly in a low fluorescence state (see below).

### Fluorescent spots of Rh/Alexa594 detected by single-molecule imaging

Fig. 1a shows a typical TIRFM image of Rh/Alexa594 in asolectin liposomes. The typical time courses of fluorescence changes for fluorescent spots are shown in Figs. 1b, 1c, and Movie S1. The interconversion between high fluorescence state ($F_{high}$) and low

fluorescence state ($F_{low}$) is immediately apparent. Fluorescence intensity steps were detected by a laboratory-written program based on a hidden Markov model (black lines in Figs. 1b and 1c). Fluorescence changes owing to blinking of the fluorophore, migration of liposome, instrumental noise etc., were excluded manually (Fig. S2).

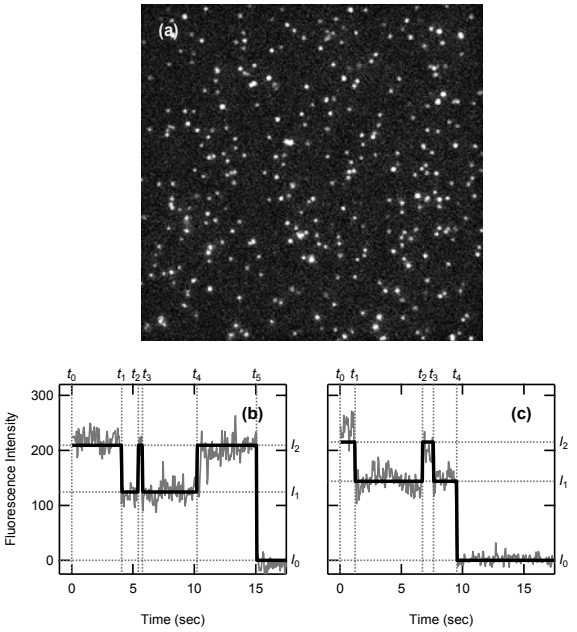


Figure 1 Typical fluorescent spots of Rh/Alexa594 observed by TIRFM. (a) A typical TIRFM image. The images were obtained at 20 frames/sec. The background was subtracted by a Rolling Ball Background Subtraction in ImageJ. (b, c) Analysis of fluorescence intensity of the fluorescent spot. The fluorescence intensity was estimated by averaging 12×12 pixels square containing a fluorescent spot. The average intensity of five 12×12 pixels squares in which no spot existed was subtracted as the background. Fluorescence intensity steps were detected by using a laboratory-written program based on a hidden Markov model (black line). See also Movie S1.

**Fluorescence intensity of single Rh/Alexa594 molecule**

It has been reported that rhodopsin has a significant tendency to form dimers in proteoliposomes (27, 28). Therefore, we examined the fluorescence intensity of a single Alexa594 molecule bound to rhodopsin to discriminate between monomers and oligomers. The histogram of the maximum fluorescence intensity ($I_2$ in Figs. 1b and 1c) was constructed from the time course of fluorescent spots (Fig. 2a). As each spot may contain one, two, or more Rh/Alexa594 molecules, the histogram was fitted with a sum of three Gaussian functions having stepwise mean values as follows:

$$A(I) = A_1 e^{\frac{(I-\mu)^2}{2\sigma^2}} + A_2 e^{\frac{(I-2\mu)^2}{4\sigma^2}} + A_3 e^{\frac{(I-3\mu)^2}{6\sigma^2}} \qquad \text{Eq. 1}$$

where $I$ is a maximum fluorescence intensity of each spot, $\mu$ is the mean intensity for a single molecule, $A_i$ ($i$=1, 2, 3) is the frequency at $i\mu$, and $i\sigma^2$ is the variance of each distribution. Using Eq. 1, the histogram of the maximum fluorescence intensity was fitted with mean

intensity $\mu$=154 for a single molecule. Furthermore, the last fluorescence decrease, corresponding to the photobleaching of the last Alexa594 molecule in each fluorescent spot was examined. Since the photobleaching of Alexa594 in $F_{high}$ (Fig. 1b) and $F_{low}$ (Fig. 1c) occurred, the histograms of the last fluorescence decrease were separately constructed (Figs. 2b and 2c, respectively). In addition, histogram for the fluorescent spots which were photobleached before the fluorescence alternation was constructed, where we could not determine which state of Alexa594 photobleached (Fig. 2d). These histograms showed the single Gaussian distributions with $\mu$=160, 126, and 145 (Figs. 2b-2d, respectively). The good agreement between $\mu$ of maximum intensity (Fig. 2a) and the photobleaching of $F_{high}$ (Fig. 2b) confirmed that most of the spots in asolectin liposomes originated from single Rh/Alexa594 molecules. Since $\mu$ varied between the measurements, we chose the spots having the maximum intensity ($I_2$) of $\mu$ ± half width half maximum ($\mu - \sqrt{2\ln 2}\,\sigma < I_2 < \mu + \sqrt{2\ln 2}\,\sigma$) for further analysis.

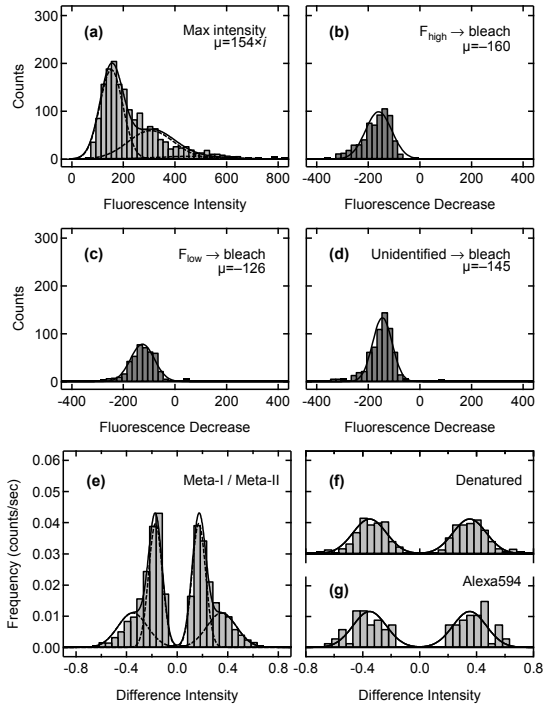


**Figure 2** Histograms of fluorescence intensity of spots and difference intensity observed by TIRFM. (a) Histograms of maximum intensity in asolectin liposomes at pH 6 ($n$=1850) fitted with three Gaussian functions shown in Eq. 1 (μ=154, σ=45, $A_1$=186, $A_2$=59, $A_3$=6). (b-d) Histograms of the fluorescence decrease upon photobleaching of Alexa594 in $F_{high}$ (b), $F_{low}$ (c) and unidentified state because of photobleaching before the fluorescence alternation (d). They were fitted with the single Gaussian functions [$n$=676, $\mu$=-160, $\sigma$=51, $A$=99 for (b), $n$=471, $\mu$=-126, $\sigma$=46, $A$=78 for (c), and $n$=703, $\mu$=-145, $\sigma$=38, $A$=134 for (d)]. (e-g) Difference intensity histograms for photo-activated rhodopsin ($n$=924) (e), denatured rhodopsin ($n$=505) (f), and free Alexa594 molecules in solution ($n$=129) (g). The difference intensity histogram in (e) was well fitted with two mirror-imaged pairs of Gaussian functions (Eq. 2: $\mu_1$=±0.304, $\sigma_1$=0.111, $A_1$=0.014 and $\mu_2$=±0.167, $\sigma_2$=0.049, $A_2$=0.037), while those in (f) and (g) were fitted with a single mirror-imaged pair of Gaussian functions [$\mu$=±0.344, $\sigma$=0.112, $A$=0.011 (f) and $\mu$=±0.377, $\sigma$=0.127, $A$=0.011 (g)].

**Fluorescence changes of single photo-activated rhodopsin molecules**

The histograms of the photobleaching of $F_{high}$ and $F_{low}$ showed that $\mu$ of $F_{low}$ (-126) was ~80% of that of $F_{high}$ (-160) (Figs. 2b and 2c). This is consistent with the ratio of the fluorescence increases for formation of Meta-II (pH 6) and Meta-I (pH 9) in bulk fluorescence measurement (Fig. S1d), showing the consistency between the bulk measurement and the single-molecule measurement. The histograms of difference fluorescence intensity (e.g. $I_1$-$I_2$ for $t_1$ and $t_3$, and $I_2$-$I_1$ for $t_2$ and $t_4$ in Fig. 1b) were constructed, in which the difference fluorescence intensities were normalized by the maximum fluorescence intensity of each spot (Figs. 2e-g). Thus the abscissa of these histograms shows the difference intensities relative to the maximum intensity of each spot. The difference intensity histogram of photo-activated rhodopsin (Fig. 2e) was fitted with the sum of two mirror-imaged pairs of Gaussian functions as follows:

$$A(\Delta I) = A_1 e^{\frac{(\Delta I+\mu_1)^2}{2{\sigma_1}^2}} + A_1 e^{\frac{(\Delta I-\mu_1)^2}{2{\sigma_1}^2}} + A_2 e^{\frac{(\Delta I+\mu_2)^2}{2{\sigma_2}^2}} + A_2 e^{\frac{(\Delta I-\mu_2)^2}{2{\sigma_2}^2}} \qquad \text{Eq. 2}$$

where $\Delta I$ is the relative difference intensity, $\mu_i$ is the mean difference, $A_i$ is the frequency at $\mu_i$, and $\sigma_i$ is the standard deviation of the $i$th distribution. The results demonstrated that the difference intensity histogram of photo-activated rhodopsin was well fitted with Eq. 2 ($\mu_1$=0.304 and $\mu_2$=0.167) (Fig. 2e).

To examine whether or not these fluorescence changes were derived from conformational changes of rhodopsin, denatured rhodopsin and free Alexa594 molecules in solution were subjected to the same TIRFM imaging and analyses (Figs. 2f and 2g). The difference intensity histogram of denatured Rh/Alexa594 was fitted with a single mirror-imaged pair of small Gaussian curves ($\mu$=±0.344) (Fig. 2f). Similar pair of small Gaussian peaks were observed in the histogram of free Alexa594 molecules ($\mu$=±0.377) (Fig. 2g). These components (noise component) likely originate from the instrumental noise and/or intrinsic fluorescence fluctuation of Alexa594, and represent the false-detection rate of conformational change in our experimental setup and analytical software. Therefore, the smaller peaks of photo-activated rhodopsin ($\mu_1$=±0.304) correspond to the noise components, whereas greater ones ($\mu_2$=±0.167) were derived from the conformational changes (Fig. 2e). It should be noted that the frequency at $\Delta I$=~0 is almost 0 because small fluorescence changes were hardly detected by our program based on hidden Markov model.

While hidden Markov model provided the most likely number of states (~3.5 states including bleached state in average), we assumed two conformational states ($F_{high}$ and $F_{low}$) because the fluorescence changes from the conformational changes were expressed by a single mirror-imaged pair of Gaussian curves at $\mu_2$=±0.167.

**Duration time after fluorescence increase or decrease in photo-activated rhodopsin**

The above results showed that the Gaussian distributions of fluorescence changes at

$\mu$=±0.167 for photo-activated rhodopsin (Fig. 2e) were due to conformational changes. In order to kinetically characterize the conformational equilibrium, we next extracted changes with difference intensity ($\Delta I$) of $\mu$ ± half width half maximum (0.167±0.058). We estimated the duration time of each conformation of photo-activated rhodopsin (e.g. $t_1$-$t_0$, $t_3$-$t_2$, and $t_5$-$t_4$ for $F_{high}$, $t_2$-$t_1$ and $t_4$-$t_3$ for $F_{low}$ in Fig. 1b), and constructed a probability histogram of duration times ($d$) of $F_{low}$ and $F_{high}$ with a bin-width of 100 ms (Figs. 3a-3d). Assuming an exponential decay of $F_{low}$ and $F_{high}$ with rate constants of $k_{low}$ and $k_{high}$, respectively, duration time histograms for $F_{low}$ and $F_{high}$ can be expressed with a single-exponential function with $k_{low}$ and $k_{high}$ as follows:

$$P_{\mathrm{low}}(d) = C_{\mathrm{low}}\exp(-k_{\mathrm{low}}d)$$
$$P_{\mathrm{high}}(d) = C_{\mathrm{high}}\exp\left(-k_{\mathrm{high}}d\right) \qquad \text{Eq. 3}$$

where $P_{low}(d)$ and $P_{high}(d)$ are the probabilities that $F_{low}$ and $F_{high}$ are converted at $d$ and $C_{low}$ and $C_{high}$ are amplification constants for $F_{low}$ and $F_{high}$, respectively. Because the decay of $F_{high}$ is caused by the conversion from $F_{high}$ to $F_{low}$ or photobleaching of Alexa594, $k_{high}$ is expressed as follows:

$$k_{\mathrm{high}} = k_{\mathrm{high}\rightarrow\mathrm{low}} + k_{\mathrm{bleach}} \qquad \text{Eq. 4}$$

where $k_{high→low}$ and $k_{bleach}$ are the rate constants for the conversion from $F_{high}$ to $F_{low}$ and photobleaching of Alexa594, respectively. Similarly, $k_{low}$ is expressed as follows:

$$k_{\mathrm{low}} = k_{\mathrm{low}\rightarrow\mathrm{high}} + k_{\mathrm{bleach}} \qquad \text{Eq. 5}$$

Duration time histograms were fitted with Eq. 3 to obtain $k_{low}$ and $k_{high}$. Using $k_{bleach}$ obtained by the single-exponential fitting of the histogram of the fluorescence retention time (e.g. $t_5$-$t_0$ in Fig. 1b), $k_{high→low}$ and $k_{low→high}$ were calculated (Table S1).

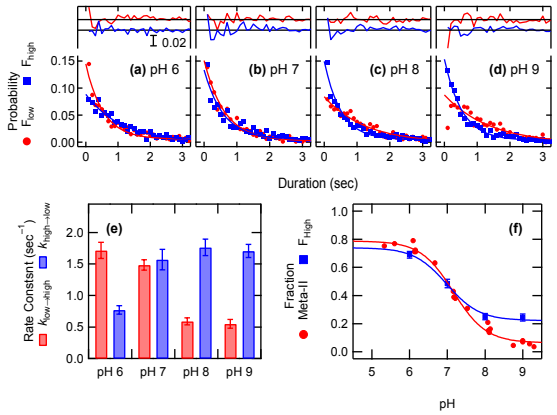


**Figure 3** Duration times for $F_{high}$ and $F_{low}$ in photo-activated rhodopsin. Histograms of duration time after fluorescence increase ($F_{high}$, blue squares) and decrease ($F_{low}$, red circles) at pH 6 (a), pH 7 (b), pH 8 (c), and pH 9 (d). Plots were fitted with a single-exponential function, and the residuals of the fit are shown above. Rate constants for conformational changes ($k_{low\rightarrow high}$ or $k_{high\rightarrow low}$) were obtained according to Eqs. 4 and 5 (Table S1). (e) pH dependency of $k_{low\rightarrow high}$ (red) and $k_{high\rightarrow low}$ (blue). (f) pH dependency of the ratio of $F_{high}$ (blue square) and Meta-II (red circle). The ratio of Meta-II was determined by UV-visible absorption measurements. Data were fitted with a Henderson-Hasselbalch equation ($f = \frac{A}{1+10^{\mathrm{pH}-\mathrm{p}K_a}} + B$). p$K_a$ was 7.16 for Meta-I/Meta-II (red), and 6.98 for $F_{low}/F_{high}$ (blue).

The pH-dependency of $k_{high\rightarrow low}$ and $k_{low\rightarrow high}$ are shown in Fig. 3e. Using these values, the pH-dependency of the ratio of $F_{high}$ was calculated (Table S1), which is consistent with the result of bulk fluorescence measurement. The profile of the pH-dependency is similar to that of the ratio of Meta-I and Meta-II estimated by UV-visible absorption spectroscopy, indicating that $F_{low}$ and $F_{high}$ essentially correspond to Meta-I and Meta-II, respectively. However, they showed a small but notable deviation at pH <6 and considerable differences at pH >8 (Fig. 3f). UV-visible absorption measurement monitors the protonation state of the Schiff base linkage, while Alexa594 at Cys316 is sensitive to the conformation around the cytoplasmic surface. Because Meta-I is favored at higher pH, greater fraction of $F_{high}$ than that of Meta-II at pH >8 suggests that Meta-I is in a mixture of $F_{high}$ and $F_{low}$. These results suggest that, Meta-I which has a protonated Schiff base linkage can partially adopt an active (open) conformation. Similarly, the small deviation between $F_{low}/F_{high}$ and Meta-I/Meta-II at pH <6 suggests that Meta-II, in which the Schiff base linkage is deprotonated, partially adopts an inactive (close) conformation.

Previous analyses have proposed an activation sequence consisting of an equilibrium between Meta-I and multiple states of Meta-II (Meta-$II_a$, Meta-$II_b$ and Meta-$II_bH^+$) (29, 30). Although Meta-$II_a$, Meta-$II_b$ and Meta-$II_bH^+$ all have a deprotonated retinal Schiff base, the conformational changes for Meta-$II_a$ formation are significantly smaller than those for Meta-$II_b$ and Meta-$II_bH^+$ (31). Thus, $F_{low}$ and $F_{high}$ of Meta-II may correspond to Meta-$II_a$ and Meta-$II_b$, respectively. Under our experimental condition (6°C), however, Meta-II is predominantly in Meta-$II_bH^+$ form (30). Our results therefore suggested that the protein

moiety of Meta-$II_bH^+$ is intrinsically interconverted between $F_{high}$ and $F_{low}$ conformations.

**Correlation between frequencies of conformational changes and G protein activation efficiencies**

Bulk fluorescence measurements showed that fluorescence intensities of dark-state rhodopsin and opsin are significantly smaller than that of photo-activated rhodopsin (Fig. S1d). However, opsin (32-35) or constitutively active mutants of rhodopsin (36-38) have low G protein activation efficiency, suggesting that dark-state rhodopsin and opsin could generate G protein activating state with low frequency. Therefore, we analyzed the fluorescence changes of dark-state rhodopsin and opsin in single molecules, to assess the possible conformational equilibrium.

Because the excitation laser for TIRFM caused the photolysis of rhodopsin, the $C_{11}$=$C_{12}$ double bond of the chromophore was fixed in the 11-*cis* configuration by the 7-membered ring retinal (7m-Ret) (19, 20) for the measurements of the dark-state rhodopsin (7m-Rh) (Fig.4a, inset). It is possible that the structural constraint of ring retinal influences the conformation or dynamics of rhodopsin. However, 7-membered ring is relatively flexible, and the circular dichroism of the chromophore of 7m-Rh is similar to that of native rhodopsin (20). In addition, the absorption spectrum of 7m-Rh is also similar to native rhodopsin. These findings suggest that the 7m-Ret, which would function as an inverse-agonist, is accommodated to the chromophore binding pocket similarly to the native 11-*cis*-retinal. The time courses of fluorescence intensity for 7m-Rh and opsin were obtained by TIRFM images and analyzed in the same manner as that for photo-activated rhodopsin to generate the respective intensity change histograms (Figs. 4a and 4d). In addition, the photo-activated rhodopsin in DMPC liposome, in which conformational change is arrested at the Meta-I stage (Fig. S1f, inset) (21), was also analyzed (Fig. 4b). The bulk fluorescence measurement showed that the fluorescence increase upon the formation of Meta-I in DMPC liposomes was ~5% (Fig. S1f). This value is significantly smaller than that of Meta-I in asolectin liposomes (~10%, Fig. S1d, pH 9), indicating that the conformational equilibrium of Meta-I in DMPC liposomes (Meta-$I^{DMPC}$) is biased to $F_{low}$ as compared to that in asolectin liposomes.

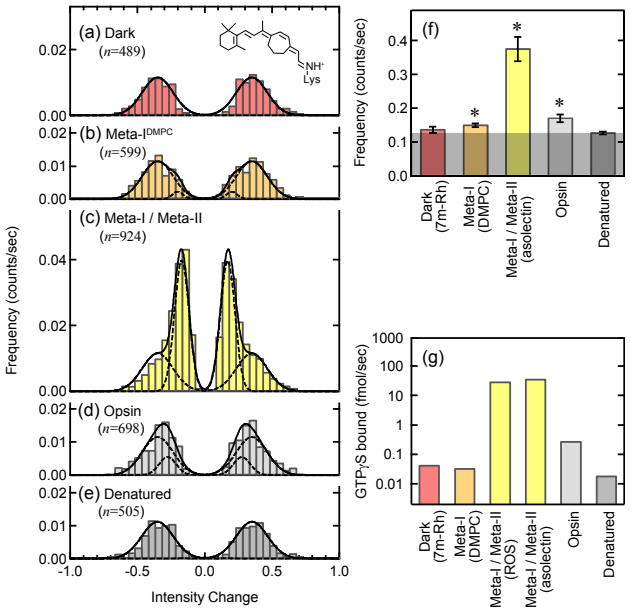


**Figure 4** Correlation between frequencies of conformational changes and G protein activation efficiencies. Intensity change histograms for dark-state (7m-Rh) (a), Meta-I in DMPC liposome (b), Meta-I/Meta-II mixture in asolectin liposomes (c), opsin (d), and denatured rhodopsin (e). These histograms were fitted with two mirror-imaged pairs of Gaussian curves (Eq. 2), where the parameters for noise components were global ($\mu_1$=0.346, $\sigma_1$=0.113, $A_1$=0.012). Additional components were observed for Meta-I$^{DMPC}$ ($\mu_2$=0.201, $\sigma_2$=0.041, $A_2$=0.002), Meta-I/Meta-II ($\mu_2$=0.171, $\sigma_2$=0.054, $A_2$=0.040), and opsin ($\mu_2$=0.279, $\sigma_2$=0.072, $A_2$=0.005). (f) The frequency of fluorescence changes obtained by the summations of difference intensity histogram. Error bar indicates the standard deviation of two to five independent datasets. Frequency for the noise component is shown by shade. The asterisk indicates that the difference from denatured rhodopsin is significant ($p$<0.05; Student's t test, two-tailed). (g) G protein activation efficiencies estimated by GTPγS binding assay.

Fluorescence changes between $F_{high}$ and $F_{low}$ occurred with a significantly lower frequency in the dark-state, Meta-I$^{DMPC}$, opsin, or denatured rhodopsin than in photo-activated rhodopsin (Meta-I/Meta-II mixture) (Figs. 4a-4e). These difference intensity histograms were global-fitted with the sum of two mirror-imaged pairs of Gaussian functions (Eq. 2), where the parameters for the noise component ($\mu_1$, $\sigma_1$ and $A_1$) were set as global variables. The excellent result of the global fitting indicates that the quantity of the noise component was equal among the histograms in Fig. 4. The histogram of dark-state (7m-Rh) and denatured rhodopsin agreed with the noise component which represents the frequency of false detection of conformational changes (Figs. 4a and 4e). On the other hand, an additional Gaussian distribution was required to reproduce the histograms for opsin and Meta-I$^{DMPC}$, indicating that conformational changes occur in these states. However, the intensity of the Gaussian distribution for conformational change of Meta-I$^{DMPC}$ and opsin (Figs. 4b and 4d) was significantly smaller than that of photo-activated rhodopsin (Fig. 4c). The percentages of the occurrence of fluorescence changes derived from conformational changes of Meta-I$^{DMPC}$ and opsin were estimated to be 6% and 27% of total occurrence of fluorescence changes, respectively. Due to this low occurrence of conformational changes, the retention times of $F_{low}$ and $F_{high}$ of opsin and Meta-I$^{DMPC}$ could not be reliably estimated. However,

when we compared the frequencies of fluorescence changes by calculating the summations of these histograms (Fig. 4f), we found that the frequencies of fluorescence changes for Meta-$I^{DMPC}$ and opsin were significantly higher than that of the dark-state or denatured rhodopsin. These results indicate that not only photo-activated rhodopsin but also Meta-$I^{DMPC}$ and opsin exhibited conformational interconversions between $F_{low}$ and $F_{high}$.

Unlike Meta-I, Meta-II, and opsin, 7m-Rh did not show fluorescence changes due to conformational changes. It is important to note that frequency of fluorescence change in each state (Fig. 4f) was consistent with the fluorescence increase observed in bulk measurements. Radionucleotide filter-binding assay showed that G protein activation efficiency of opsin was 1/100 of that of photo-activated rhodopsin in asolectin liposomes, whereas those of 7m-Rh and Meta-$I^{DMPC}$ were negligible (Fig. 4g). This tendency is consistent with the frequency of fluorescence changes as well. These findings suggested that the active state ($F_{high}$) is accumulated by the increase of $k_{low\rightarrow high}$ rather than the decrease of $k_{high\rightarrow low}$ (see Discussion).

## DISCUSSION

In this study, we observed the conformational changes of single rhodopsin molecules using Alexa594 as a fluorescent probe. We first monitored the conformational dynamics in single photo-activated rhodopsin molecules. The fluorescence intensity alternated between $F_{high}$ and $F_{low}$, which are likely to correspond to active and inactive conformations, respectively. Such fluorescence alternation was also observed in the denatured rhodopsin and free Alexa594 molecule, implying that the fluorescence intensity steps detected by our analysis included stochastic noise and/or intrinsic fluorescence fluctuation of Alexa594 as well as conformational changes. However, the excellent result of global fitting of histograms of fluorescence changes with two mirror-imaged pairs of Gaussian distributions, in which the parameters for the noise component were global, demonstrated that the quantity of noise component was equal in all samples and the frequency of fluorescence changes derived from the conformational changes was quantitatively evaluated (Fig. 4).

When the fluorescence spots having $\Delta I$ within 0.167 ± 0.058 were chosen in photo-activated rhodopsin in asolectin liposome (Fig. 2e), the occurrence of fluorescence changes derived from conformational changes was significantly greater than that from noise components (Figs. 2f and 2g). Thus the dynamics of the equilibrium between $F_{high}$ and $F_{low}$ was examined in detail for photo-activated rhodopsin. The difference between the pH-dependent profile of absorption (Meta-I/Meta-II, Fig. 3f, red) and fluorescence ($F_{low}/F_{high}$, Fig. 3f, blue) measurements indicates that Meta-I as well as Meta-II are not in a uniform conformation, but they are in an equilibrium between active and inactive conformations. Using the acidic and alkaline values obtained by fitting the absorption and fluorescence data with Henderson-Hasselbalch equation and assuming that the pH-dependency of the ratio of $F_{high}$ to $F_{low}$ within Meta-I and Meta-II are negligible, the fractions of $F_{high}$ in Meta-I and

Meta-II were calculated to be 0.18 and 0.89, respectively. Therefore, Gibbs free energy difference ($\Delta G$) for the formation of the active state ($= -RT\ln\frac{F_{high}}{F_{low}}$) is +3.6 kJ/mol when the ligand is a protonated all-*trans*-retinal (Meta-I), whereas $\Delta G$ is -4.9 kJ/mol when the ligand is a deprotonated all-*trans*-retinal (Meta-II) (Fig. 5), implying that the disruption of the ionic lock by the deprotonation of the chromophore decreases $\Delta G$ by 8.5 kJ/mol. Note that the conformation of Meta-I$^{DMPC}$ is biased to $F_{low}$ and $\Delta G$ would be greater than that for Meta-I in asolectin liposomes.

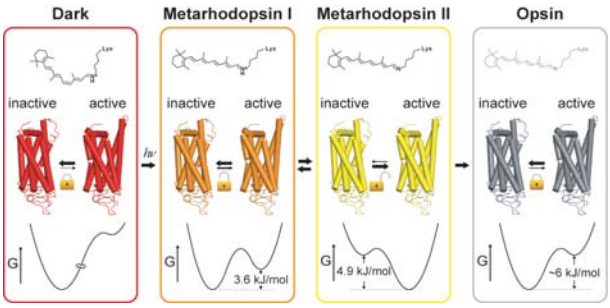


**Figure 5** Activation mechanism of rhodopsin based on ligand-induced population shift. Meta-I, Meta-II, opsin and possibly dark state rhodopsin are in the equilibria between active and inactive conformations. Agonist all-*trans* retinal shifts the equilibrium toward active conformation by depressing $\Delta G$, whereas inverse agonist 11-*cis* retinal shifts the equilibrium toward inactive conformation by elevating $\Delta G$. Note that $\Delta G$ for Meta-I$^{DMPC}$ would be greater than that for Meta-I in asolectin liposomes.

We have shown that the conformational equilibrium within individual photo-activated rhodopsin molecules can be observed by single-molecule analysis. Using this method, we then measured the possible conformational equilibrium in the dark state, opsin, and Meta-I$^{DMPC}$, which are thought to be single species. We found that while no fluorescence changes other than noise component were observed for the dark-state rhodopsin (containing 7m-Ret), Meta-I$^{DMPC}$ and opsin exhibited clear fluorescence changes, albeit with smaller frequency than photo-activated rhodopsin (Fig. 4f). In addition, Meta-I and Meta-II in asolectin liposome are also in the equilibrium between $F_{low}$ and $F_{high}$, as shown by the deviation of pH-dependence between $F_{low}/F_{high}$ and Meta-I/Meta-II (Fig. 3f), indicating that rhodopsin molecule intrinsically adopts both active and inactive conformation. Interestingly, the frequencies of conformational changes correlated with the fluorescence increase observed in bulk measurements and the G protein activation efficiencies (Fig. 4g). G protein activity should linearly correlate with the fraction of $F_{high}$ in the mixture of $F_{low}$ and $F_{high}$ ($= \frac{F_{high}}{F_{low}+F_{high}} = \frac{k_{low\to high}}{k_{high\to low}+k_{low\to high}}$), whereas frequency of fluorescence changes is given by the sum of frequency from $F_{low}$ to $F_{high}$ ($= \frac{k_{high\to low}}{k_{high\to low}+k_{low\to high}} \times k_{low\to high}$) and that from $F_{high}$ to

$F_{low}$ ($= \frac{k_{low \to high}}{k_{high \to low} + k_{low \to high}} \times k_{high \to low}$). These equations imply that the fraction of $F_{high}$ is increased by the increase of $k_{low \to high}$ or the decrease of $k_{high \to low}$, while the increases of $k_{low \to high}$ and $k_{high \to low}$ both result in the increase of frequency of fluorescence changes. Therefore, it is suggested that the active state ($F_{high}$) is accumulated by the increase of $k_{low \to high}$ rather than the decrease of $k_{high \to low}$. Rhodopsin is locked in the inactive conformation mainly by an ionic lock between Arg134 in the conserved ERY motif (Helix 3) and Glu247 (Helix 6). It is proposed that this ionic lock is coupled with the ionic bond between protonated Schiff base of the chromophore and its counterion Glu113 (Helix 3) (39, 40), which is replaced by the ionic bond between Glu113 and Lys296 in opsin. Our current findings of the presence of $F_{high}$ and $F_{low}$ within one species suggest that the ionic lock and chromophore are not strictly coupled. Because Alexa594 is likely to be sensitive to the disruption of the ionic lock, the rate of the disruption of the ionic lock would be regulated by the presence/absence, configuration, or the protonation state of the chromophore.

FTIR experiments have suggested that opsin adopts a Meta-II-like conformation at acidic pH (p$K_a$=4.1) (41), however the amount of active conformation would be quite low in our experimental condition (pH 6-9) (41). In addition, crystal structure of opsin was similar to that of Meta-II (42), while the structure of C-terminal ~20 amino acid residues was not resolved. These findings suggest that the conformation of $F_{high}$ of opsin is similar to $F_{high}$ of the photo-activated rhodopsin. However, the difference in the fluorescence intensities between $F_{high}$ and $F_{low}$ (mean difference intensity, $\mu$) for opsin ($\mu$=±0.279) was greater than that for photo-activated rhodopsin ($\mu$=±0.171) (Figs. 4d and 4c). This difference suggests that the difference in local conformations between $F_{high}$ of Meta-II and that of opsin around Cys316 may be one of the reasons why the relation between the frequency and the G protein activation efficiency was not linear. The bulk fluorescence measurements demonstrated that the fluorescence increase upon formation of opsin is ~60% of that of Meta-I (Fig. S1d, pH 9.0). If two-state equilibrium of opsin, similar to that of Meta-I, is assumed and the difference in μ is taken into consideration, $\Delta G$ of opsin is calculated to be ~6 kJ/mol (Fig. 5).

Unlike Meta-I, Meta-II, and opsin, fluorescence alternation due to the conformational changes was not observable for dark-state rhodopsin (7m-Rh). This suggests that conformational conversion to $F_{high}$ is suppressed by binding to 11-*cis*-retinal which functions as an inverse agonist. It is known that the extremely low G protein activation efficiency of dark state rhodopsin accounts for the low dark noise of rod cells so as to function as a single photon detector. Low G protein activation efficiency of the dark state rhodopsin is explained by the low rate of thermal isomerization of the chromophore, but it would be also caused by the suppression of the generation of $F_{high}$.

Our current results demonstrate that the conformational dynamics between $F_{low}$ and $F_{high}$ is essential for the activation and inactivation of rhodopsin. The retinal chromophore changes its potency from inverse-agonist to agonist through photo-isomerization. In agreement with

the potency of the ligand, the $\Delta G$ between active and inactive conformations is changed and the equilibrium is shifted (Fig. 5). The ligand-induced population shift during the activation process of rhodopsin substantiates the conceptual two-state model which can explain characteristic biological responses of GPCRs to several pharmacologically distinguishable ligands (43-46).

The present single-molecule study successfully monitored the dynamics within individual rhodopsin molecules and quantitatively analyzed these conformational equilibria. Accumulated evidence about crystal structures of GPCRs revealed that the helical arrangements of active and inactive conformations in rhodopsin are similar to those in other GPCRs. The present single-molecule analysis using a fluorophore-labeled receptor molecule is applicable to the evaluation of conformational fluctuation of active and inactive states in a variety of GPCRs. Further combination of these two techniques would accelerate extending the theoretical framework of activation to better explain drug behavior.

## SUPPORTING MATERIAL

Characterization of Rh/Alexa594 in ROS membrane, asolectin liposome, and DMPC liposome (Figure S1), false detections of fluorescence change points (Figure S2), kinetic parameters (Table S1), and typical TIRFM images and fluorescence time courses (Movie S1) are available at http://www.biophysj.org/biophysj/supplemental/.....

## ACKNOWLEDGEMENTS

We are grateful to Dr. Koji Nakanishi at Columbia University for provision of the 11-*cis*-locked 7-membered ring retinal. We thank Dr. Yoshinori Fujiyoshi at Nagoya University for technical support and helpful discussion. We also thank Dr. Takesi Matsuyama at Kyoto University for critical reading of our manuscript and invaluable comments. This work was supported by the Japanese Ministry of Education, Culture, Sports, Science and Technology (MEXT) [Grants-in-Aid for Scientific Research to T. Y. (25440167), Y. Shichida (25251036, 60127090), and Y. I. (23370070), and Grants for Excellent Graduate Schools].

## REFERENCES

1. Shichida, Y., and H. Imai. 1998. Visual pigment: G-protein-coupled receptor for light signals. *Cell Mol. Life Sci.* 54:1299-1315.
2. Kandori, H., Y. Shichida, and T. Yoshizawa. 2001. Photoisomerization in rhodopsin. *Biochemistry (Mosc)* 66:1197-1209.
3. Hofmann, K. P. 1985. Effect of GTP on the rhodopsin-G-protein complex by transient formation of extra metarhodopsin II. *Biochim. Biophys. Acta* 810:278-281.
4. Choe, H. W., Y. J. Kim, J. H. Park, T. Morizumi, E. F. Pai, N. Krauss, K. P. Hofmann, P. Scheerer, and O. P. Ernst. 2011. Crystal structure of metarhodopsin II. *Nature* 471:651-655.
5. Standfuss, J., P. C. Edwards, A. D'Antona, M. Fransen, G. Xie, D. D. Oprian, and G. F. Schertler. 2011. The structural basis of agonist-induced activation in constitutively active rhodopsin. *Nature* 471:656-660.
6. Rasmussen, S. G., H. J. Choi, J. J. Fung, E. Pardon, P. Casarosa, P. S. Chae, B. T. Devree, D. M. Rosenbaum, F. S. Thian, T. S. Kobilka, A. Schnapp, I. Konetzki, R. K. Sunahara, S. H. Gellman, A. Pautsch, J. Steyaert, W. I. Weis, and B. K. Kobilka. 2011. Structure of a nanobody-stabilized active state of the $\beta_2$ adrenoceptor. *Nature* 469:175-180.
7. Rasmussen, S. G., B. T. DeVree, Y. Zou, A. C. Kruse, K. Y. Chung, T. S. Kobilka, F. S. Thian, P. S. Chae, E. Pardon, D. Calinski, J. M. Mathiesen, S. T. Shah, J. A. Lyons, M. Caffrey, S. H. Gellman, J. Steyaert, G. Skiniotis, W. I. Weis, R. K. Sunahara, and B. K. Kobilka. 2011. Crystal structure of the $\beta_2$ adrenergic receptor-Gs protein complex. *Nature* 477:549-555.
8. Struts, A. V., G. F. Salgado, K. Martinez-Mayorga, and M. F. Brown. 2011. Retinal dynamics underlie its switch from inverse agonist to agonist during rhodopsin activation. *Nat Struct Mol Biol* 18:392-394.
9. Angel, T. E., S. Gupta, B. Jastrzebska, K. Palczewski, and M. R. Chance. 2009. Structural waters define a functional channel mediating activation of the GPCR, rhodopsin. *Proc. Natl. Acad. Sci. U. S. A.* 106:14367-14372.
10. Orban, T., B. Jastrzebska, S. Gupta, B. Wang, M. Miyagi, M. R. Chance, and K. Palczewski. 2012. Conformational dynamics of activation for the pentameric complex of dimeric G protein-coupled receptor and heterotrimeric G protein. *Structure* 20:826-840.
11. Ye, S., T. Huber, R. Vogel, and T. P. Sakmar. 2009. FTIR analysis of GPCR activation using azido probes. *Nat. Chem. Biol.* 5:397-399.
12. Kozuka, J., H. Yokota, Y. Arai, Y. Ishii, and T. Yanagida. 2006. Dynamic polymorphism of single actin molecules in the actin filament. *Nat. Chem. Biol.* 2:83-86.

13. Arai, Y., A. H. Iwane, T. Wazawa, H. Yokota, Y. Ishii, T. Kataoka, and T. Yanagida. 2006. Dynamic polymorphism of Ras observed by single molecule FRET is the basis for molecular recognition. *Biochem. Biophys. Res. Commun.* 343:809-815.
14. Teramura, Y., J. Ichinose, H. Takagi, K. Nishida, T. Yanagida, and Y. Sako. 2006. Single-molecule analysis of epidermal growth factor binding on the surface of living cells. *EMBO J.* 25:4215-4222.
15. Hiroshima, M., Y. Saeki, M. Okada-Hatakeyama, and Y. Sako. 2012. Dynamically varying interactions between heregulin and ErbB proteins detected by single-molecule analysis in living cells. *Proc. Natl. Acad. Sci. U. S. A.* 109:13984-13989.
16. Hibino, K., T. Shibata, T. Yanagida, and Y. Sako. 2011. Activation kinetics of RAF protein in the ternary complex of RAF, RAS-GTP, and kinase on the plasma membrane of living cells: single-molecule imaging analysis. *J. Biol. Chem.* 286:36460-36468.
17. Matthews, R. G., R. Hubbard, P. K. Brown, and G. Wald. 1963. Tautomeric forms of metarhodopsin. *J. Gen. Physiol.* 47:215-240.
18. Imamoto, Y., M. Kataoka, F. Tokunaga, and K. Palczewski. 2000. Light-induced conformational changes of rhodopsin probed by fluorescent Alexa594 immobilized on the cytoplasmic surface. *Biochemistry* 39:15225-15233.
19. Mao, B., M. Tsuda, T. G. Ebrey, H. Akita, V. Balogh-Nair, and K. Nakanishi. 1981. Flash photolysis and low temperature photochemistry of bovine rhodopsin with a fixed 11-ene. *Biophys. J.* 35:543-546.
20. Akita, H., S. P. Tanis, M. Adams, V. Baloghnair, and K. Nakanishi. 1980. Non-bleachable rhodopsins retaining the full natural chromophore. *J. Am. Chem. Soc.* 102:6370-6372.
21. Baldwin, P. A., and W. L. Hubbell. 1985. Effects of lipid environment on the light-induced conformational changes of rhodopsin. 1. Absence of metarhodopsin II production in dimyristoylphosphatidylcholine recombinant membranes. *Biochemistry* 24:2624-2632.
22. Yamashita, T., A. Terakita, and Y. Shichida. 2000. Distinct roles of the second and third cytoplasmic loops of bovine rhodopsin in G protein activation. *J. Biol. Chem.* 275:34272-34279.
23. Rabiner, L. R. 1989. A tutorial on hidden Markov models and seleceted applications in speech recognition. *Proc. IEEE* 77:257-286.
24. Bronson, J. E., J. Fei, J. M. Hofman, R. L. Gonzalez, Jr., and C. H. Wiggins. 2009. Learning rates and states from biophysical time series: a Bayesian approach to model selection and single-molecule FRET data. *Biophys. J.* 97:3196-3205.
25. Parkes, J. H., and P. A. Liebman. 1984. Temperature and pH dependence of the metarhodopsin I-metarhodopsin II kinetics and equilibria in bovine rod disk membrane suspensions. *Biochemistry* 23:5054-5061.

26. Sato, K., T. Morizumi, T. Yamashita, and Y. Shichida. 2010. Direct observation of the pH-dependent equilibrium between metarhodopsins I and II and the pH-independent interaction of metarhodopsin II with transducin C-terminal peptide. *Biochemistry* 49:736-741.
27. Mansoor, S. E., K. Palczewski, and D. L. Farrens. 2006. Rhodopsin self-associates in asolectin liposomes. *Proc. Natl. Acad. Sci. U. S. A.* 103:3060-3065.
28. Fotiadis, D., B. Jastrzebska, A. Philippsen, D. J. Müller, K. Palczewski, and A. Engel. 2006. Structure of the rhodopsin dimer: a working model for G-protein-coupled receptors. *Curr. Opin. Struct. Biol.* 16:252-259.
29. Knierim, B., K. P. Hofmann, O. P. Ernst, and W. L. Hubbell. 2007. Sequence of late molecular events in the activation of rhodopsin. *Proc. Natl. Acad. Sci. U. S. A.* 104:20290-20295.
30. Mahalingam, M., K. Martinez-Mayorga, M. F. Brown, and R. Vogel. 2008. Two protonation switches control rhodopsin activation in membranes. *Proc. Natl. Acad. Sci. U. S. A.* 105:17795-17800.
31. Zaitseva, E., M. F. Brown, and R. Vogel. 2010. Sequential rearrangement of interhelical networks upon rhodopsin activation in membranes: the Meta $II_a$ conformational substate. *J. Am. Chem. Soc.* 132:4815-4821.
32. Surya, A., K. W. Foster, and B. E. Knox. 1995. Transducin activation by the bovine opsin apoprotein. *J. Biol. Chem.* 270:5024-5031.
33. Jäger, S., K. Palczewski, and K. P. Hofmann. 1996. Opsin/*all-trans*-retinal complex activates transducin by different mechanisms than photolyzed rhodopsin. *Biochemistry* 35:2901-2908.
34. Han, M., J. Lou, K. Nakanishi, T. P. Sakmar, and S. O. Smith. 1997. Partial agonist activity of 11-*cis*-retinal in rhodopsin mutants. *J. Biol. Chem.* 272:23081-23085.
35. Surya, A., and B. E. Knox. 1997. Modulation of opsin apoprotein activity by retinal. Dark activity of rhodopsin formed at low temperature. *J. Biol. Chem.* 272:21745-21750.
36. Robinson, P. R., G. B. Cohen, E. A. Zhukovsky, and D. D. Oprian. 1992. Constitutively active mutants of rhodopsin. *Neuron* 9:719-725.
37. Cohen, G. B., T. Yang, P. R. Robinson, and D. D. Oprian. 1993. Constitutive activation of opsin: influence of charge at position 134 and size at position 296. *Biochemistry* 32:6111-6115.
38. Han, M., S. O. Smith, and T. P. Sakmar. 1998. Constitutive activation of opsin by mutation of methionine 257 on transmembrane helix 6. *Biochemistry* 37:8253-8261.
39. Vogel, R., T. P. Sakmar, M. Sheves, and F. Siebert. 2007. Coupling of protonation switches during rhodopsin activation. *Photochem Photobiol* 83:286-292.
40. Vogel, R., M. Mahalingam, S. Ludeke, T. Huber, F. Siebert, and T. P. Sakmar. 2008. Functional role of the "ionic lock"--an interhelical hydrogen-bond network in family A

heptahelical receptors. *J. Mol. Biol.* 380:648-655.

41. Vogel, R., and F. Siebert. 2001. Conformations of the active and inactive states of opsin. *J. Biol. Chem.* 276:38487-38493.
42. Park, J. H., P. Scheerer, K. P. Hofmann, H. W. Choe, and O. P. Ernst. 2008. Crystal structure of the ligand-free G-protein-coupled receptor opsin. *Nature* 454:183-187.
43. Lefkowitz, R. J., S. Cotecchia, P. Samama, and T. Costa. 1993. Constitutive activity of receptors coupled to guanine nucleotide regulatory proteins. *Trends Pharmacol. Sci.* 14:303-307.
44. Samama, P., S. Cotecchia, T. Costa, and R. J. Lefkowitz. 1993. A mutation-induced activated state of the $\beta_2$-adrenergic receptor. Extending the ternary complex model. *J. Biol. Chem.* 268:4625-4636.
45. Robertson, M. J., I. G. Dougall, D. Harper, K. C. W. Mckechnie, and P. Leff. 1994. Agonist-antagonist interactions at angiotensin receptors - Application of a 2-state receptor model. *Trends Pharmacol. Sci.* 15:364-369.
46. Leff, P. 1995. The two-state model of receptor activation. *Trends Pharmacol. Sci.* 16:89-97.

# Supporting Material

## Single-molecule observation of the ligand-induced population shift of rhodopsin, a G-protein coupled receptor

Ryo Maeda,[†] Michio Hiroshima,[‡,§] Takahiro Yamashita,[†] Akimori Wada,[¶] Shoko Nishimura,[‖] Yasushi Sako,[‡] Yoshinori Shichida,[†] and Yasushi Imamoto[†]

[†]Department of Biophysics, Graduate School of Science, Kyoto University, Kyoto 606-8502, Japan; [‡]Cellular Informatics Laboratory, RIKEN, 2-1 Hirosawa, Wako 351-0198, Japan; [§]Laboratory for Cell Signaling Dynamics, RIKEN Quantitative Biology Center, 6-2-3 Furuedai, Suita 565-0874, Japan; [¶]Department of Organic Chemistry for Life Science, Kobe Pharmaceutical University, Kobe 658-8558, Japan; and [‖]Cellular and Structural Physiology Institute, Nagoya University, Nagoya 464-8601, Japan.

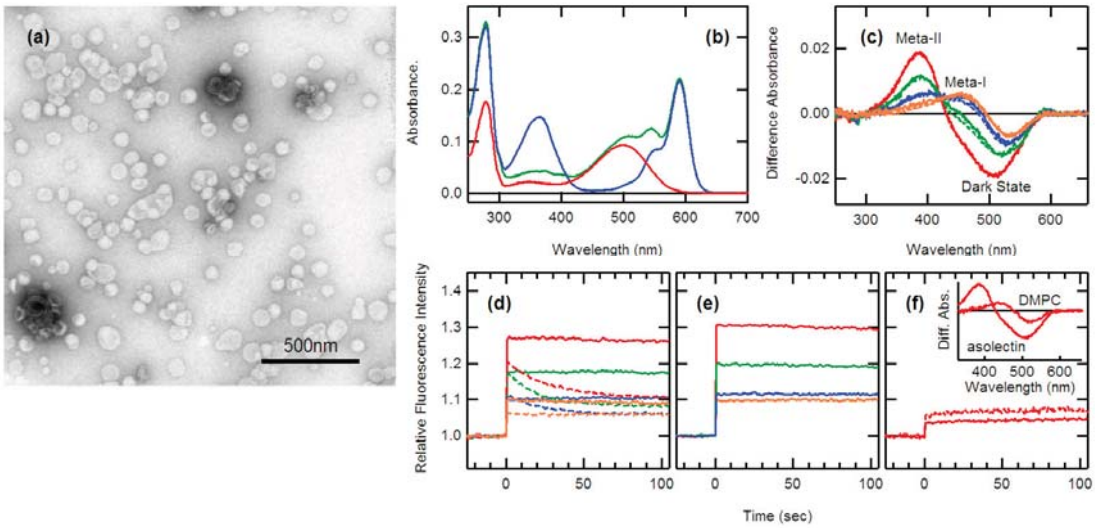


**FIGURE S1** Spectroscopic characteristics of Rh/Alexa594 in proteoliposomes. (a) An electron microscope image of asolectin liposomes. The mean diameter of liposomes was 66.4 nm. (b) Absorption spectra of purified Rh/Alexa594 before (green) and after (blue) irradiation in the presence of 50 mM hydroxylamine. The molar ratio of rhodopsin and Alexa594 was 1:0.98. The optical purity index ($Abs_{280}/Abs_{500}$) of unmodified rhodopsin purified using our protocol was 1.88 (red). (c) Light-induced spectral changes of Rh/Alexa594 in asolectin liposomes (solid line) and unlabeled rhodopsin in ROS membranes (dotted line) at pH 6 (red), pH 7 (green), pH 8 (blue), and pH 9 (orange). Each curve was obtained by subtracting the spectrum before irradiation from that 180 s after irradiation. Samples were irradiated for 1 min through Y52 cutoff filter at 6°C. (d-f) Time-course of fluorescence change of Rh/Alexa594 in asolectin liposomes (d), ROS membranes (e), and DMPC liposomes (f) at pH 6 (red), pH 7 (green), pH 8 (blue), and pH 9 (orange). All of the traces were recorded at 6°C with 500 ms time resolution. Alexa594 was excited with 605 nm light and its fluorescence was detected at 630 nm. Samples were irradiated for 10 seconds through Y52 cutoff filter at $t$ = 0 s. Broken lines show the fluorescence changes in the presence of 10 mM hydroxylamine. (inset) Light-induced spectral change of Rh/Alexa594 in DMPC liposome at pH 6, in which conformational change is arrested at the Meta-I stage, is compared to that in asolectin liposome.

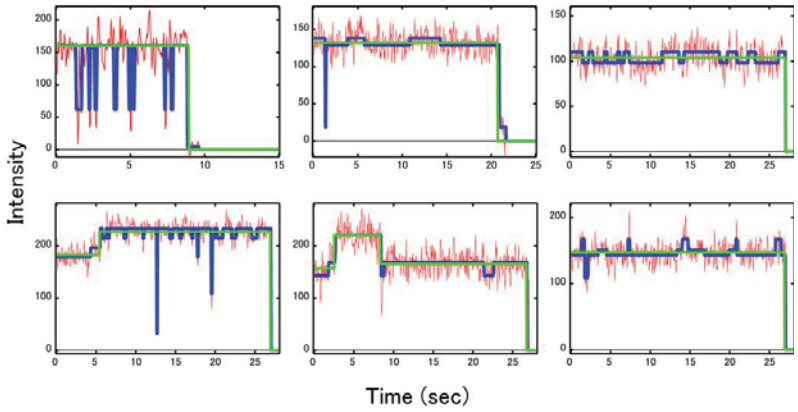


**FIGURE S2** Examples of manual removal of false detections. The fluorescence intensity steps were detected using a laboratory-written program based on a hidden Markov model (blue lines). However, some of traces included radical fluorescence changes that were likely derived from artifactual factors other than conformational changes, such as fluorophore blinking and migration of liposome (e.g. left top). In addition, frequent tiny fluorescence changes were detected in the noisy fluorescence traces containing no large fluorescence changes (e.g. right top). In some cases, one-step fluorescence change was recognized as two-step change (e.g. middle top). These "false detections" were excluded by removing short-lived changes that lasted for less than 5 frames and then by manually removing detections caused by noisy data (green lines). However, false detections could not be completely removed, and the remainder is observed as the shared noise component contained in the frequency histograms of the fluorescence changes (Figs. 2e-g and 4a-e).

**TABLE S1. Rate constants for the conversions of $F_{low}$ and $F_{high}$.**

| pH | $k_{low}$ | $k_{high}$ | $k_{bleach}$ | $k_{low \rightarrow high}$ | $k_{high \rightarrow low}$ | Ratio of $F_{high}$ |
|---|---|---|---|---|---|---|
| 6.0 | 1.85 ± 0.13 | 0.90 ± 0.07 | 0.13 ± 0.00 | 1.72 ± 0.13 | 0.77 ± 0.07 | 0.69 ± 0.02 |
| 7.0 | 1.63 ± 0.08 | 1.71 ± 0.16 | 0.14 ± 0.00 | 1.49 ± 0.08 | 1.57 ± 0.16 | 0.49 ± 0.03 |
| 8.0 | 0.80 ± 0.06 | 1.97 ± 0.13 | 0.21 ± 0.00 | 0.59 ± 0.06 | 1.76 ± 0.13 | 0.25 ± 0.02 |
| 9.0 | 0.72 ± 0.07 | 1.88 ± 0.10 | 0.17 ± 0.00 | 0.55 ± 0.07 | 1.71 ± 0.10 | 0.24 ± 0.03 |

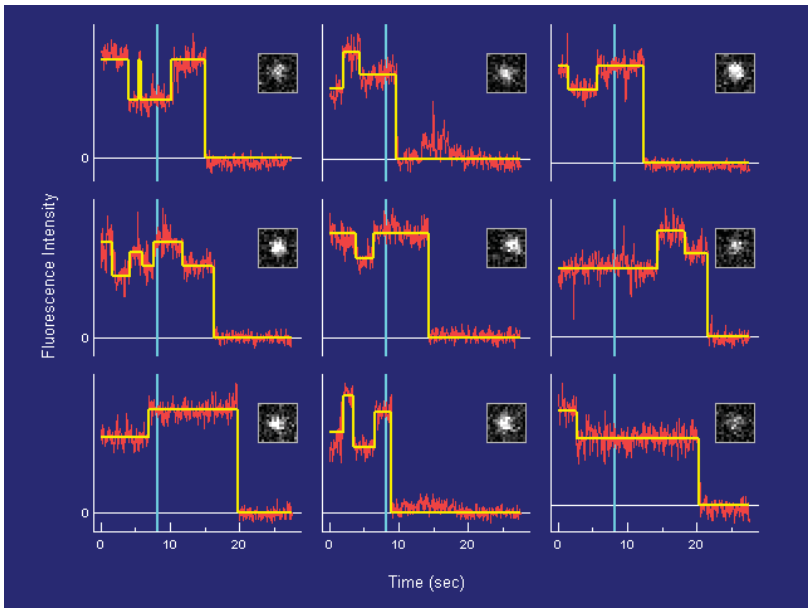


**MOVIE S1** Single-molecule images and fluorescence time course of the typical fluorescence spots shown in Fig. 1a.